CHAPTER 3

Rock Physics Analysis Results

Typically, the key well logs for a rock physics study comprise of compressional wave and shear wave velocities, and bulk density. The rock physics analysis was carried out using RokDoc software, and geophysical log data from Wells-A, -B, -C and -D were available as input to this study.

3.1 Well Log Data Conditioning

Well log data QC and conditioning were applied to improve quality and consistency of the measured data, as raw log data was used as input to this project. The quality of the well log data in this area were affected by borehole conditions, changing borehole sizes and missing sections. To ensure the high quality of the input well logs and subsequent results, bad data points were removed, and missing sections were replaced by estimated log data values. Figures 3-1 and 3-2 show the original measured logs, edited logs and predicted logs of all wells.

Unrealistic high values, observed as spikes, were removed from the sonic (Vp) log data as part of the well log data conditioning. The spikes were mostly caused by interference caused by the associated bad cement that did not provide sufficient coupling for the tool.

Data inconsistency, missing data, and poor quality measurements of density log data caused by bad borehole conditions were evident in Wells-B, -C and -D, as these were the older wells used in this study (Figure 3-3). By contrast, the borehole conditions and log data measurements were considered to be good quality in Well-A. Poor quality data were replace with synthetic log data computed using Gardner's empirical equation (Gardner et al., 1974). Synthetic density data were created using the following equations;

Limestone: $\rho = 1.176Vp^{0.0995}$ (3-4),

Shale: $\rho = 1.460Vp^{0.0690}$ (3-5),

where ρ is density in g/cm^3 and Vp is compressional wave velocity in m/s. The density logs for Well-C and Well-D were predicted from compressional wave velocity logs, using a power-law function as suggested by Gardner et al. (1974). Finally, measured density logs were spliced with the calculated density logs. The result of well conditioning showed data consistency between the wells (Figure 3-4) allowing the data to be used confidently in the following steps.

Lithology logs were predicted at all wells using gamma ray log cut-off values, combined with interpreted composite logs. The interpreted lithologies consisted mostly of carbonate (limestones, marls and calcarenite) in the shallow section, sandstone (sandstone and siltstone), and shale (shale and calcareous claystone) in the deeper section.

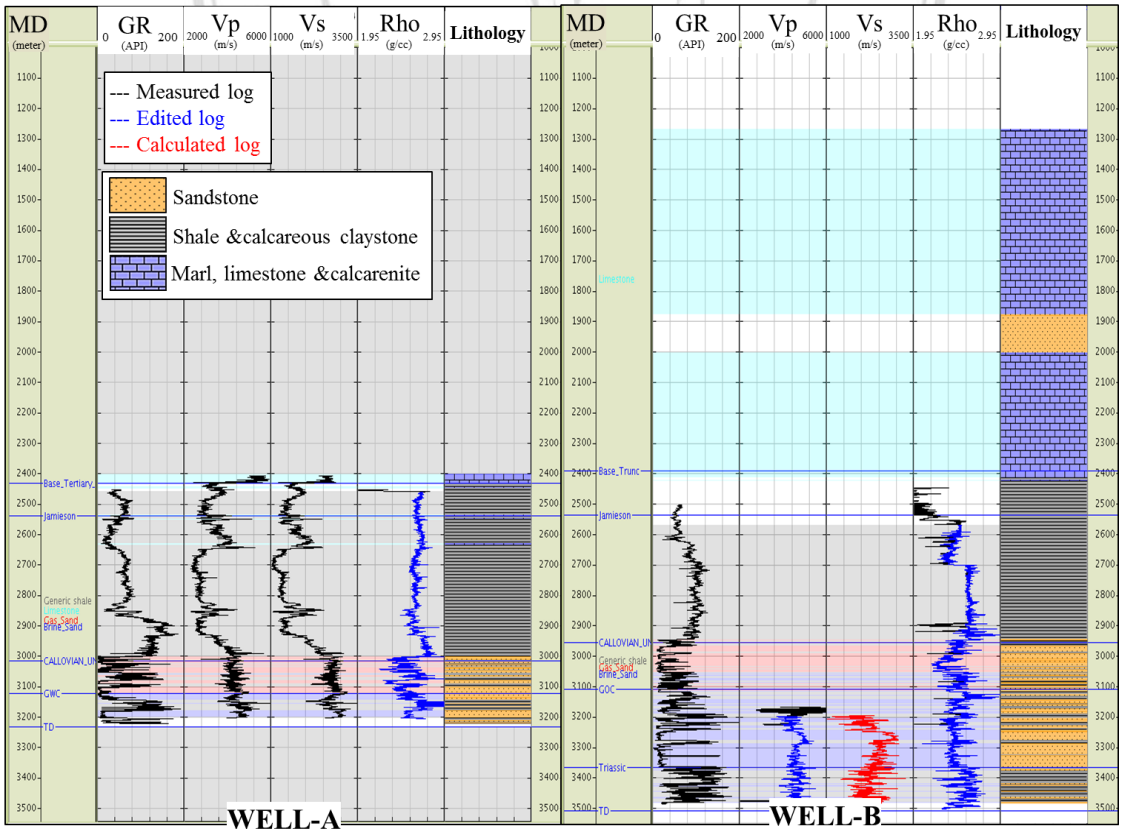

Figure 3-1 Composite well log data (measured, edited and calculated) for Wells-A and -B.

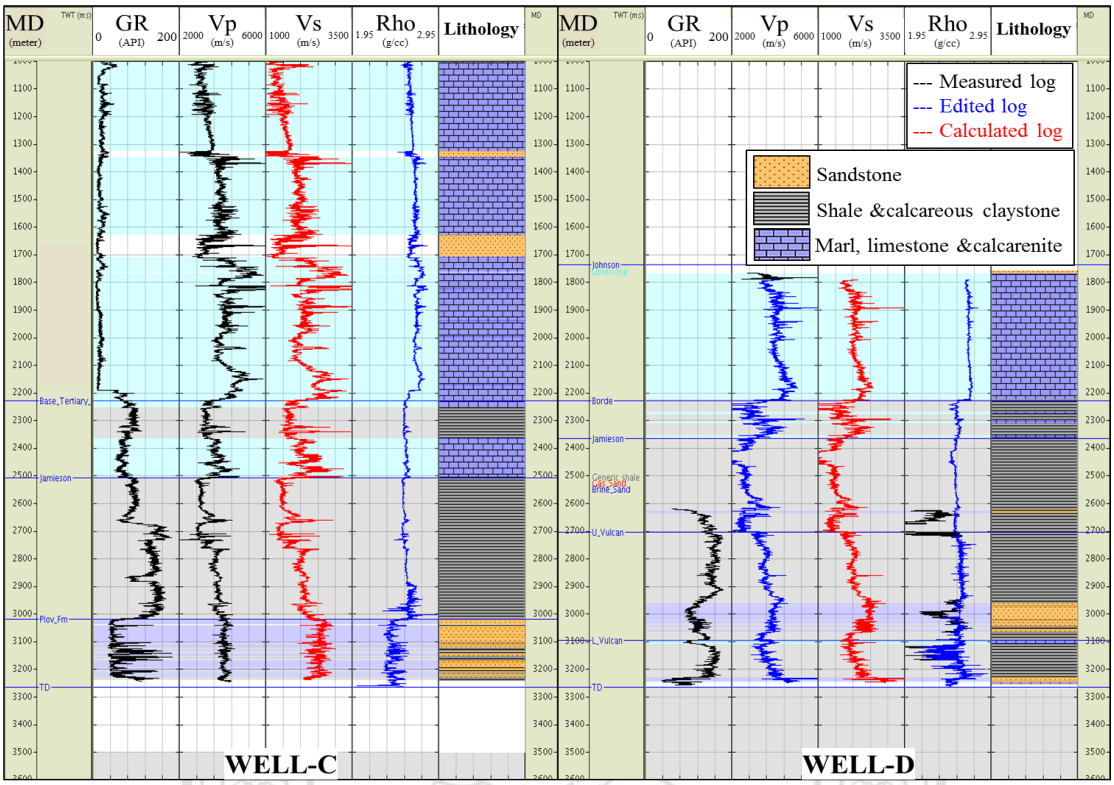

Figure 3-2 Composite well log data (measured, edited and calculated) for Wells-C and -D.

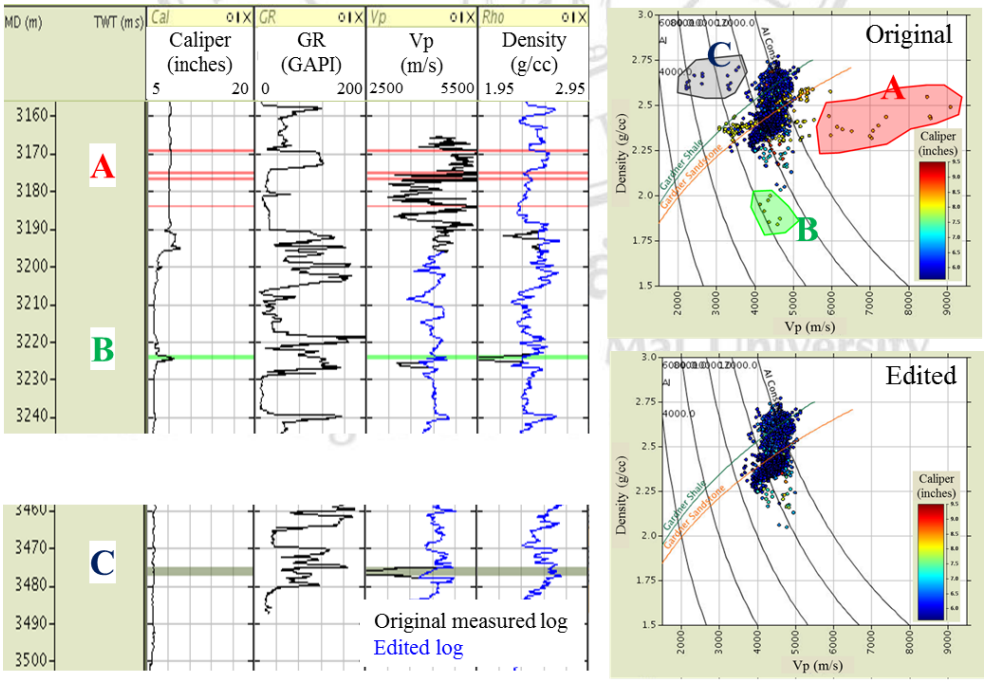

Figure 3-3 Crossplot of Vp and density in Well-B using original measured log data (top) and edited well data (bottom). Polygons-A, -B and -C were highlighted on edited data points which corresponded on log viewer.

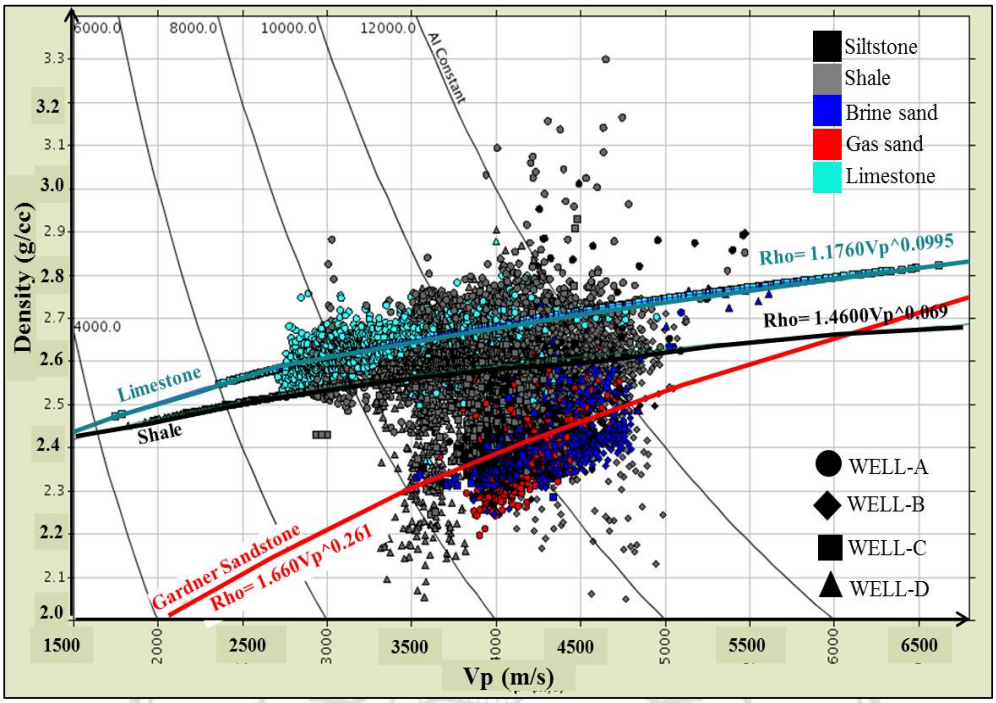

Figure 3-4 Crossplot of Vp and density log data for all wells colored by interpreted lithology log after well log data conditioning.

3.2 Shear Wave Velocity Prediction

Castagna et al. (1985) ,and Greenberg and Castagna (1992) demonstrated a correlation between Vp and Vs for most sedimentary rock types, and defined empirical relationships to calculate Vs from Vp in various brine-filled lithologies. An empiric linear relationship, based on these principles, was derived in Well-A (Figure 3-5), and applied to predict shear sonic logs for Well-B, Well-C and Well-D. The derived equations used for shear wave velocity prediction for various lithologies, such as sandstone, shale and carbonates, were defined as follows;

Sandstone: $Vs = 0.86Vp - 890$ (3-1),

Shale: $Vs = 0.79Vp - 880$ (3-2),

Carbonates: $Vs = 0.72Vp - 850$ (3-3),

where Vp represent measured compressional velocity in km/s. These relationships were applied at all wells which measured Vs log data was not available.

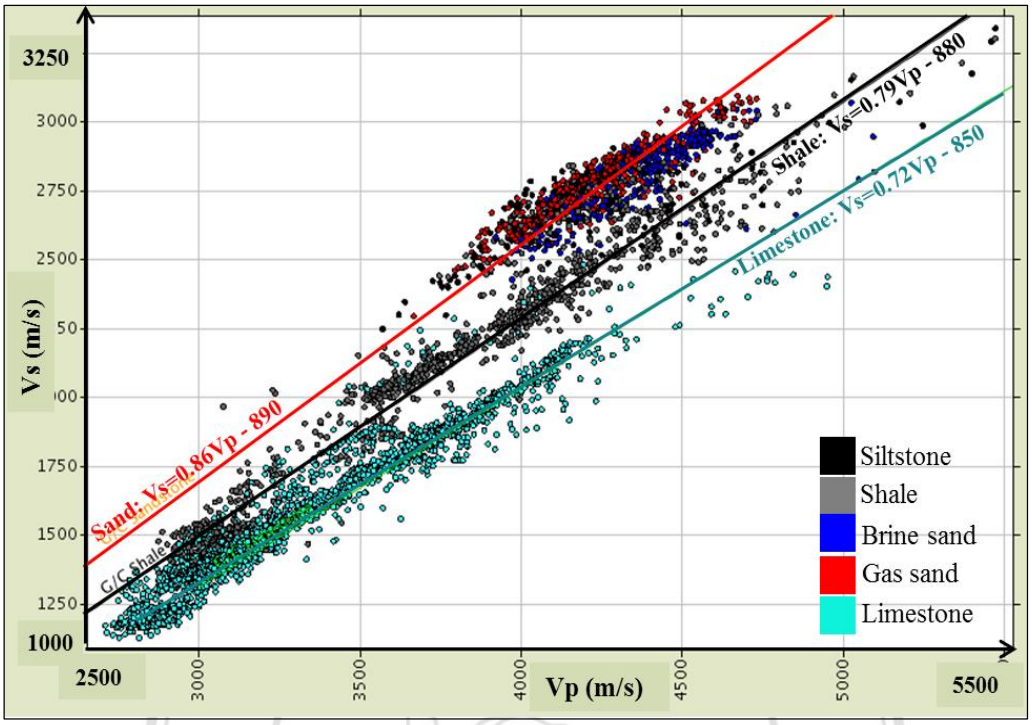

Figure 3-5 Crossplot demonstrating empirical best fit equations for Vp versus Vs using measured log data from Well-A, colored by interpreted lithology log data.

3.3 Reservoir Characterization Feasibility

The crossplot of compressional wave velocity versus effective porosity was provided to understand the rock frame stiffness and the depositional environment. The combined well log data for sandstone were all plotted together (Figure 3-6). As observation from the crossplot, the data for the four input wells were showed that they shared a similar depositional environment and rock frame properties, indicated by the overlap of the data. The crossplot also suggested that the rock frame could be characterized as relatively hard, as most of the data points plotted close to the upper Hashin-Shtrikman bound. This observation could also mean that a majority of the sandstone in the area is too hard to be sensitive to pore fluid variations, and this will be discussed further in the next paragraph.

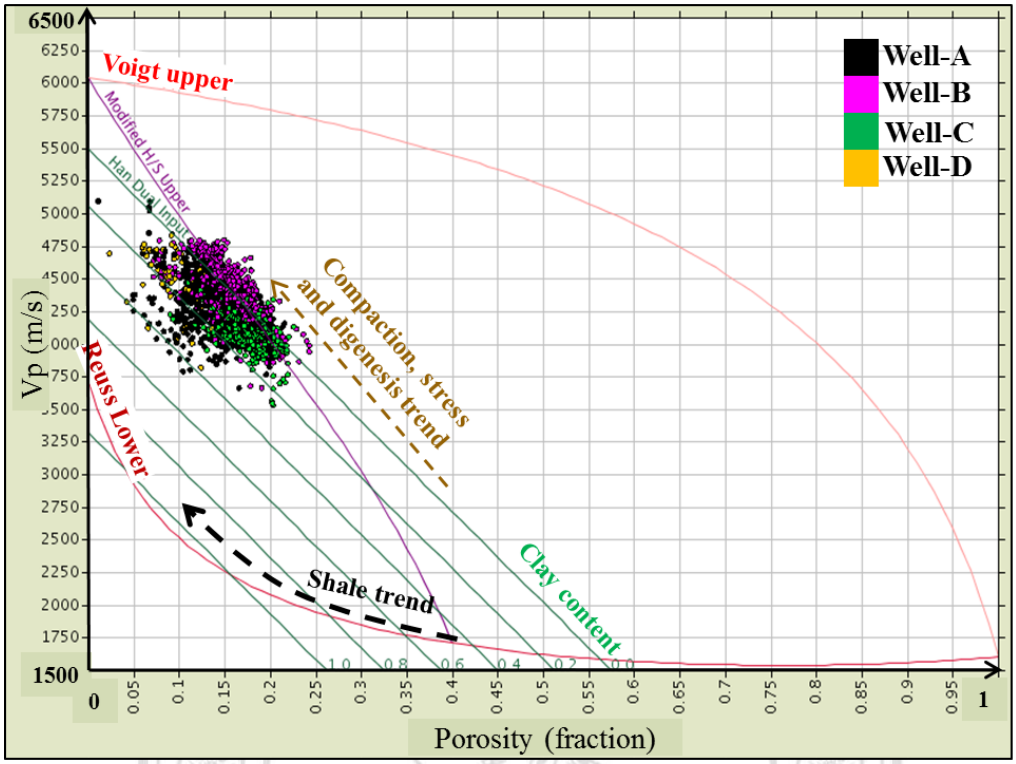

Figure 3-6 Crossplot of compressional wave velocity versus effective porosity for sandstone colored by well.

Both acoustic impedance (AI) and Vp/Vs logs were calculated for all four input wells. A crossplot of AI versus Vp/Vs clearly illustrated the importance of applying an elastic inversion workflow to achieve effective differentiation of both lithology and fluid types in this area (Figure 3-7). The crossplot showed that applying a post-stack inversion workflow to derive AI could not efficiently separate lithology or fluid types in this area. On the other hand, as shown in the crossplot, by inverting for shear impedance (SI) using a pre-stack inversion followed by Vp/Vs computation, lithology discrimination seemed feasible. However, the crossplot also indicated that it would be difficult to achieve fluid type discrimination in this area. This was believed to be due to the low porosity values and the relatively hard rock frame in the reservoir section.

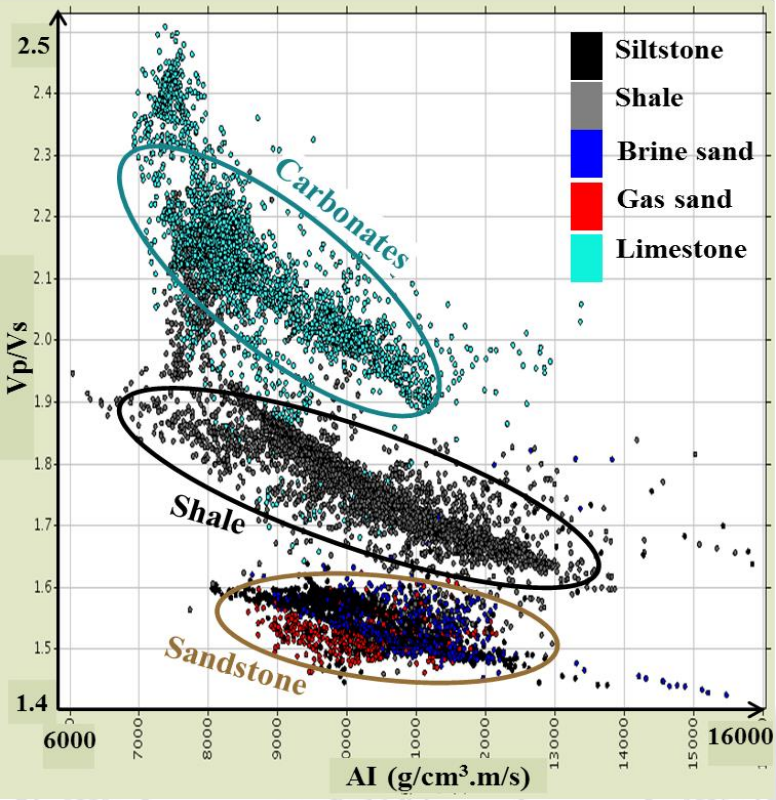

Figure 3-7 Crossplot of Vp/Vs versus acoustic impedance (AI) for Well-A colored by lithology type.

3.4 Fluid Replacement Modelling

Fluid replacement modelling (FRM) was performed for all wells and respective sandstone units. The main inputs were well log data (Vp, Vs, density and porosity), fluid properties and mineral properties, and in-situ water saturation log (Sw). Fluid properties were calculated using all necessary parameters derived from repeat formation test (RFT) data of Well-B. Mineral properties used were RokDoc software defaults (Table 3-1), originating from Mavko et al. (1998).

Table 3-1 Mineral properties input to rock physics analysis and FRM (modified after Mavko et al., 1998).

Mineral type	Bulk modulus (GPa)	Shear modulus (GPa)	Young modulus (GPa)	Density (g/cc)	Vp (m/s)	Vs (m/s)
Quartz	36.6	45	96.6	2.65	6037.62	4120.82
Shale	11.4	3	15.4	2.35	2559.92	1129.87

The RFT tool was primarily designed to measure formation pressure and collect fluid samples at specific targets in a wellbore. Based on such RFT data, pressure, temperature and fluid parameters were extracted from Well-B as follows:

Depth:	3116.0	m MD-KB,
	3095.8	m TVD-SS,
Pressure:	4442	psia,
	30.63	MPa,
Temperature:	110	˚C,
Geothermal gradient:	4.04	˚C/100 meters,
Water Salinity:	2500	ppm,
Specific gravity of gas:	0.810	(Air=1),
Gas/Oil ratio (GOR):	774	scf/BBL,
	137.8	v/v,
Oil API:	31.8	API.

The fluid properties were computed using the fluid calculator in the RokDoc software, as shown in Figure 3-8. The calculation of elastic properties for oil, gas and brine was carried out using the Batzle and Wang (1992) equations, and required input parameters for API, gas-oil ratio (GOR), gas gravity, salinity, pressure and temperature (Figure 3-8). The resulting fluid properties were summarized in Table 3-2.

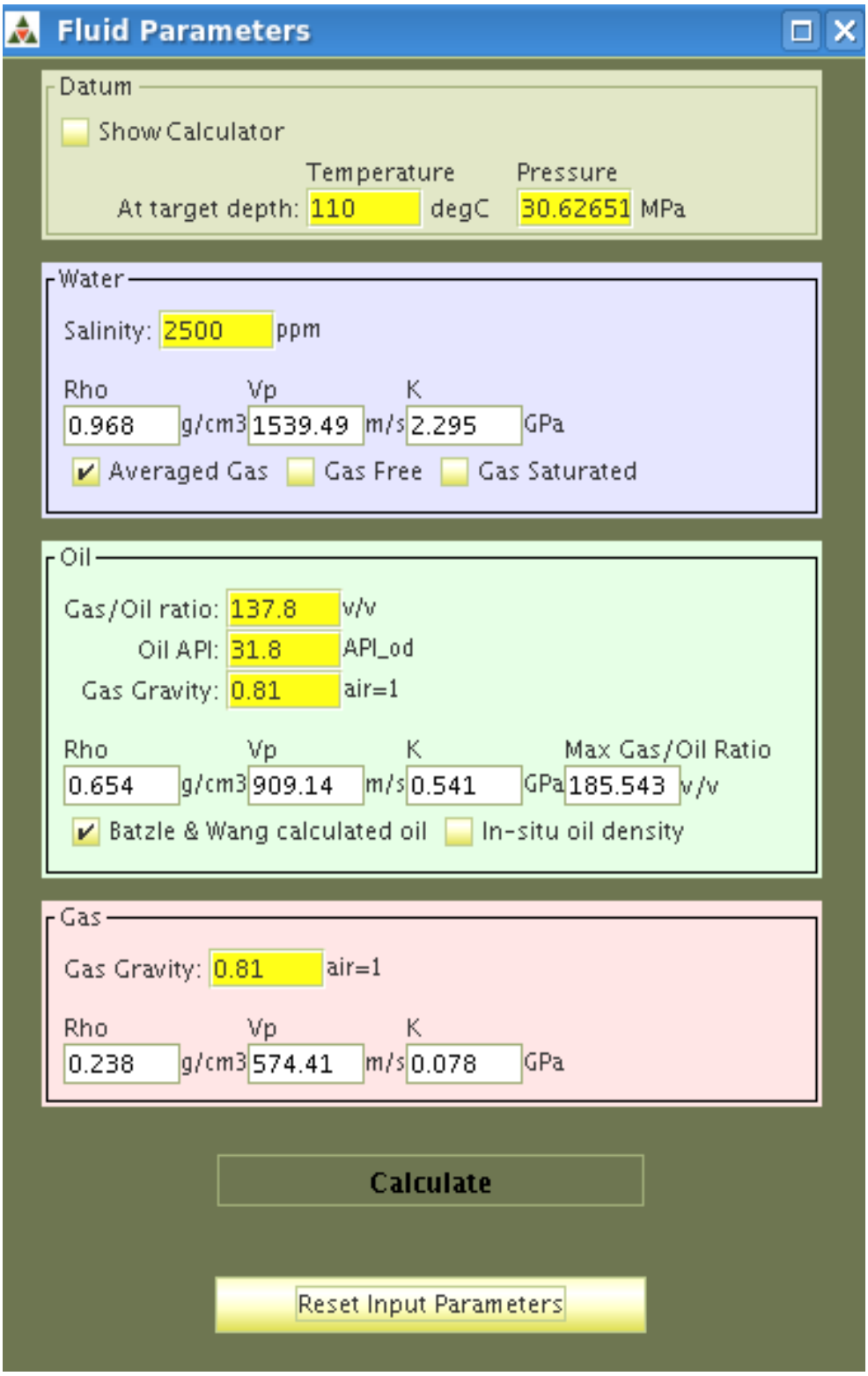

Figure 3-8 Fluid calculator in RokDoc software was used in fluid properties calculation.

Table 3-2 Fluid properties were calculated using the Batzle and Wang (1992) relationships.

Fluid type	Bulk modulus (GPa)	Shear modulus (GPa)	Density (g/cc)	Vp (m/s)	Vs (m/s)
Brine	2.294	0	0.968	1539.49	0
Oil	0.541	0	0.654	909.14	0
Gas	0.079	0	0.238	574.41	0

Under reservoir conditions the oil and gas cases are normally a mixture of oil/brine or gas/brine. In this case only two cases were considered, a brine case consisting of 100% brine, and a gas case consisting of a mixture of 80% gas and 20% brine. The elastic property of the fluid mixture was calculated using Wood's equation (Wood, 1941), which provides the weighted harmonic average of the bulk moduli of the input fluids as Table 3-3.

Table 3-3 Elastic properties of a fluid mixture of 80% gas and 20% brine.

Fluid type	Density (g/cc)	Vp (m/s)	Vs (m/s)
Gas 80% (Brine 20%)	0.384	767.43	0

A fluid sensitivity diagnostics plot was based on the ratio of the dry rock frame and matrix material bulk modulus (y-axis), combined with porosity (x-axis). As Figure 3-9 illustrates, the values derived for Well-A varied between intermediate to very hard pore stiffness. The data points in Well-B were less scattered and the pore stiffness was predominantly classified as intermediate to hard. Only a small amount of sandstone was observed in Well-D, but was classified with hard pore stiffness. Well-C was represented by the data with the softest pore stiffness in the area. Nevertheless, the results illustrated in these diagnostics plots indicated that only minor fluid sensitivities could be expected to be observed from seismic data in this area.

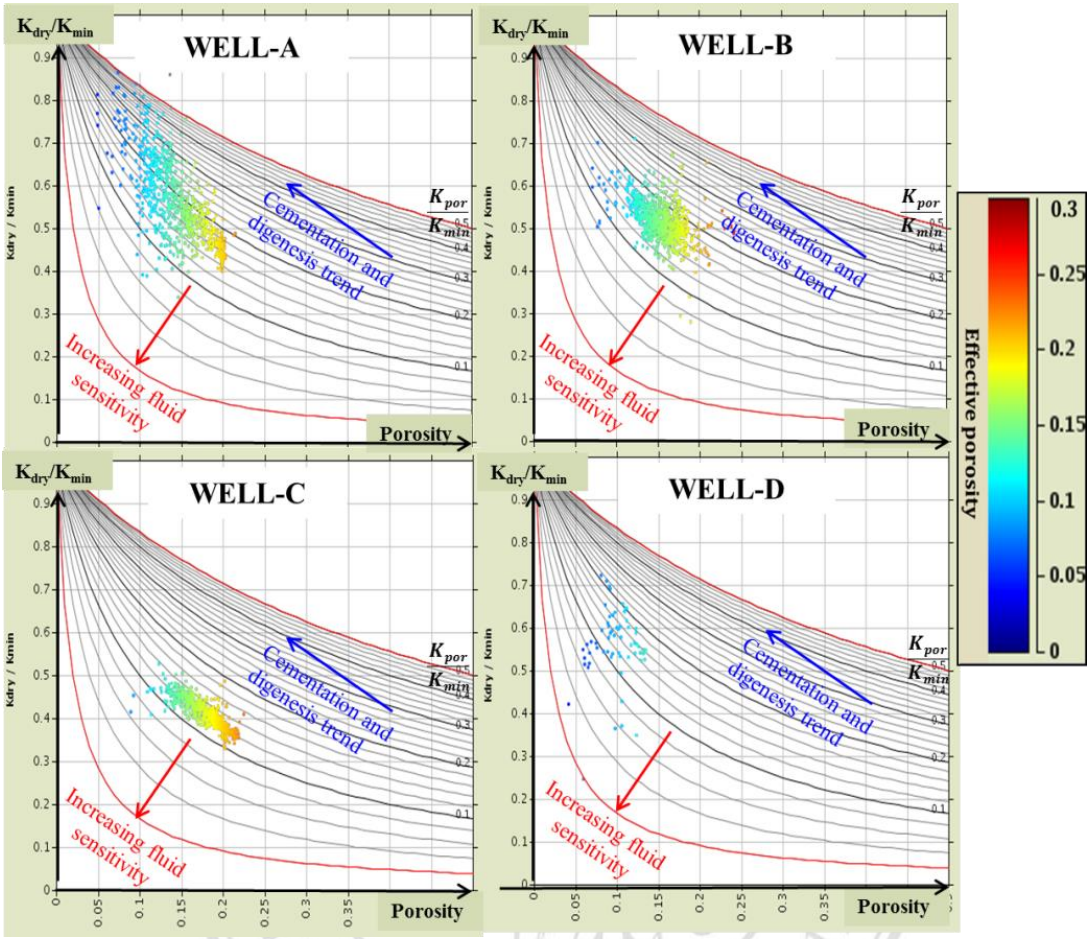

Figure 3-9 Crossplot of Kdry/Kmin versus effective porosity colored by effective porosity for each wells.

After fluid substitution, a final log set of Vp, Vs and density logs was prepared for all models (80% gas saturated sand, 100% brine saturated sand and in-situ fluid saturated sand), similar to the example of Well-A (Figure 3-10). The log sets of 80% gas saturated sand showed lower acoustic impedance (lower Vp and density), and higher Vs (small increasing of density) compared with 100% brine saturated rock. A crossplot of AI versus Vp/Vs was used to illustrate the effect of fluid variations on the porous sandstone units to visualise the effect of fluid variations to parameters derived from the elastic inversion of seismic data (Figure 3-11).

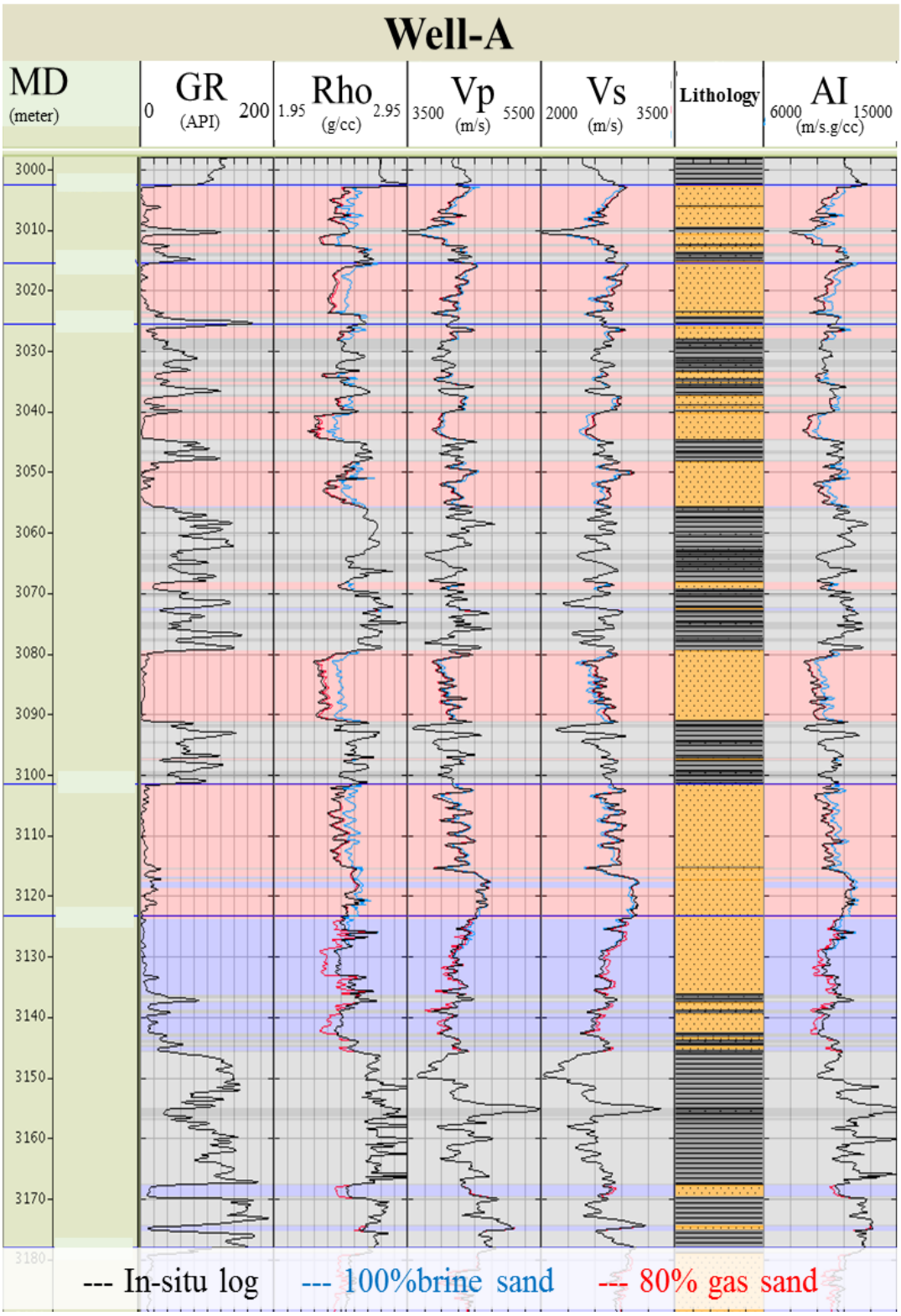

Figure 3-10 Well log plot showing the effect of FRM in Well-A.

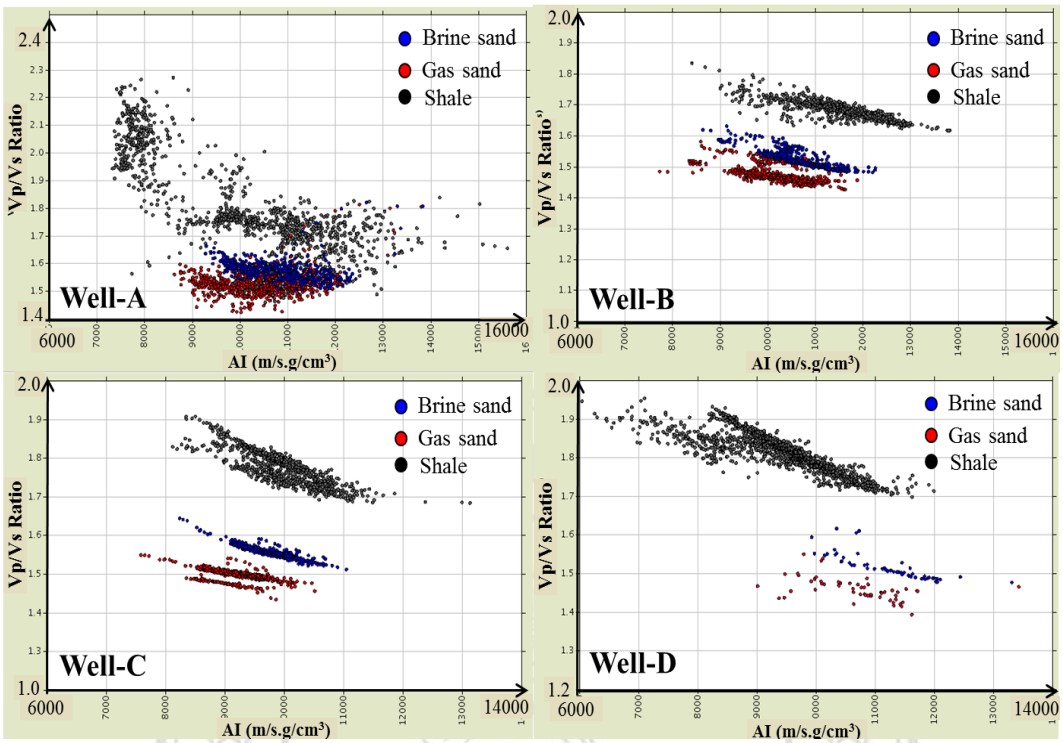

Figure 3-11 Crossplot of acoustic impedance versus Vp/Vs ratio after application of FRM for all four input wells. Trends are similar for all wells, but separation of both lithology and fluid effects were further enhanced for Wells-B, -C, and -D, probably caused by the use of a synthetic Vs log for these wells.

3.5 AVO analysis and attributes

Amplitude versus offset (AVO) was analyzed using blocky models to categorize the AVO classes based on input well log data. The analysis was considered for three cases to evaluate sensitivity to pore fluid variations, and included shale over gas sand, shale over brine sand and shale over in-situ fluid saturated sand. The input Vp, Vs and density for these cases were averaged from measured and calculated well logs (derived from FRM) (Table 3-4).

AVO analysis and attributes were carried out for all wells, using the classification scheme discussed previously (CHAPTER 2). AVO analysis plots were generated, showing the reflection coefficient (RC) versus incidence angle, intercept-gradient crossplot, Monte-Carlo simulation of interface data in intercept-gradient domain to derive weighted stack equation, and a Gaussian distribution of data points based on Monte-Carlo simulation. The analysis plot shows the near and far stack angles as red

and blue dots. Additionally, the data values related to interfaces of shale over gas sand, shale over brine sand and shale over in-situ fluid saturated sand were marked as red, blue and black data points, respectively.

The interface reflectivity calculation was carried out using Aki and Richards (1980) 3 terms approximation of the Zoeppritz equations, plotting incidence angle (θ) along the x-axis. The Aki-Richards equation considered in this case is only the downgoing P-wave and upgoing P-wave case, which says that the reflectivity at angle θ is the weighted sum of the Vp, Vs and density data. The AVO classes considered were I, II, IIp, III and IV as previously discussed in CHAPTER 2.

Table 3-4 Average values of Vp, Vs and density used in AVO analysis as input.

Well-A

Lithology	Fluid	Vp Mean (m/s)	Vs Mean (m/s)	Rho Mean (g/cc)
Generic shale		3766.86	2143.32	2.67
Sandstone	Gas80%	4263.70	2799.60	2.43
	Water100%	4312.21	2752.22	2.51
	In-situ	4280.85	2787.03	2.45

Well-B

Lithology	Fluid	Vp Mean (m/s)	Vs Mean (m/s)	Rho Mean (g/cc)
Generic shale		4498.87	2674.11	2.55
Sandstone	Gas80%	4381.08	2974.79	2.31
	Water100%	4437.77	2918.56	2.40
	In-situ	4429.75	2919.59	2.40

Well-C

Lithology	Fluid	Vp Mean (m/s)	Vs Mean (m/s)	Rho Mean (g/cc)
Generic shale		3892.18	2194.82	2.56
Sandstone	Gas80%	4011.12	2678.92	2.28
	Water100%	4088.45	2625.11	2.38
	In-situ	4087.46	2625.22	2.38

Well-D

Lithology	Fluid	Vp Mean (m/s)	Vs Mean (m/s)	Rho Mean (g/cc)
Generic shale		3701.13	2043.90	2.56
Sandstone	Gas80%	4011.12	2678.92	2.28
	Water100%	4622.15	3079.86	2.54
	In-situ	4616.34	3080.06	2.54

AVO classification results of each interface at wells were defined using combination of four plots (Figure 3-12) which comprised (a) the AVO analysis plot (reflectivity versus incident angle), (b) intercept and gradient crossplot, (c) Monte-Carlo

simulation of intercept-gradient at interface with weighted stack function and (d) Weight stack of intercept-gradient based on Monte-Carlo simulation.

The weighted stack equation applied to each interfaces is shown on the weight stack plot. AVO values that fall on the line will have a weighted stack value of zero. This method also ensures that a particular AVO response is isolated, and can be easily identified. The formula is:

$$WS = mI + c - G \quad (3\text{-}6),$$

where m is slope of the weighted stack line, c is intercept of the weighted stack line on the y-axis, I is intercept value and G is the gradient value.

The AVO attribute analysis for Wells-A, -B, -C and -D can be seen in Figures 3-12 to 3-15. The analysis showed that the AVO classification varied from well to well, which could be caused by different burial depths or mineralogical variations in the area. A summary of the AVO classification can be seen in Table 3-5. These observations were as expected, considering the results obtained in the Section 3-4. However, the AVO classification remained insensitive to changing pore fluids, with the exception of the ambiguous results derived in Well-C. The results derived at Well-C indicate that fluid variations may affect the AVO classification, but it is believed that these results were influenced by the use of modeled Vs data during FRM and Section 3-4 was presented softest pore stiffness data (lower Kdry/Kmin comparing each other wells). Based on these observations, it is therefore believed that fluid fill variations would be very challenging to detect from seismic amplitude data.

Table 3-5 Summary of AVO classification.

Well name	AVO classes		
	In-situ sand	Brine sand	Gas sand
Well-A	IIp	IIp	IIp
Well-B	III	III	III
Well-C	II/III	II/III	III
Well-D	IIp	IIp	IIp

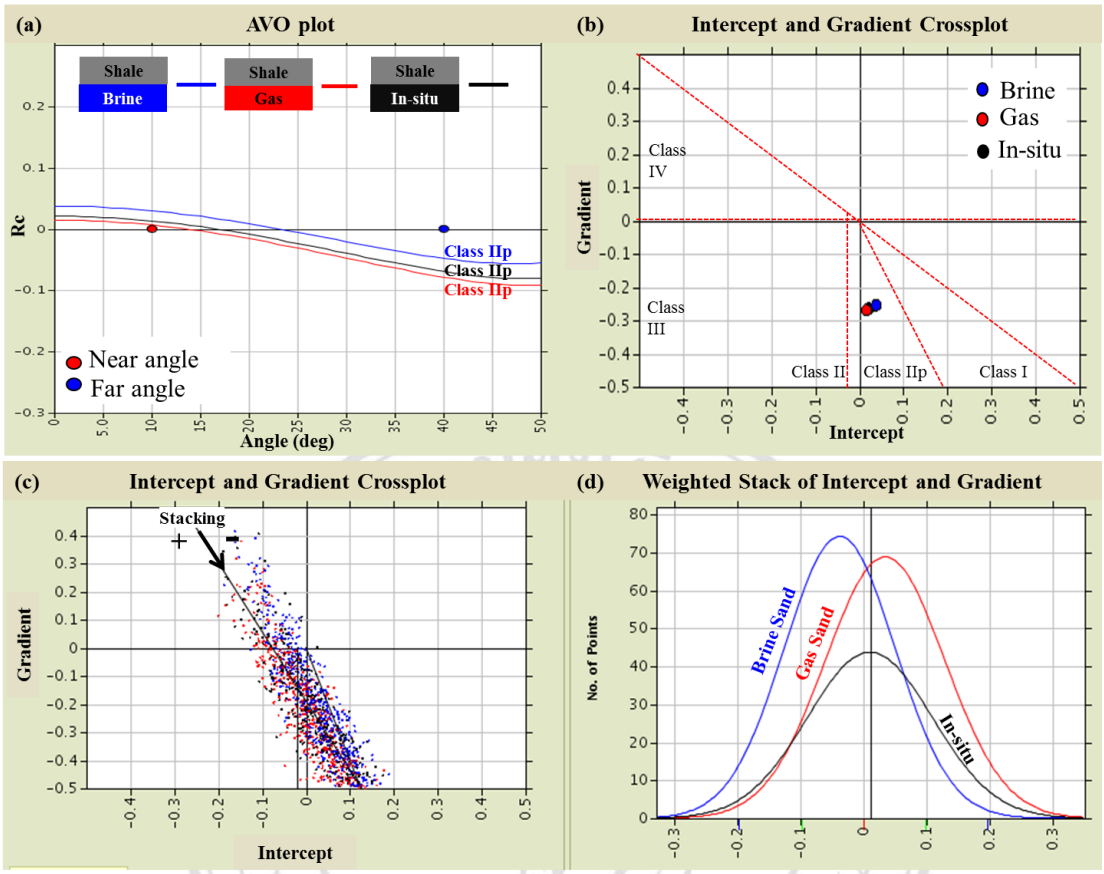

Figure 3-12 The plots using Well-A models for AVO classification comprised (a) AVO analysis plots showing RC versus incidence angle, (b) intercept-gradient crossplot, (c) Monte-Carlo simulation of intercept-gradient at interface with weighted stack function, and (d) Gaussian distribution of data points based on Monte-Carlo simulation.

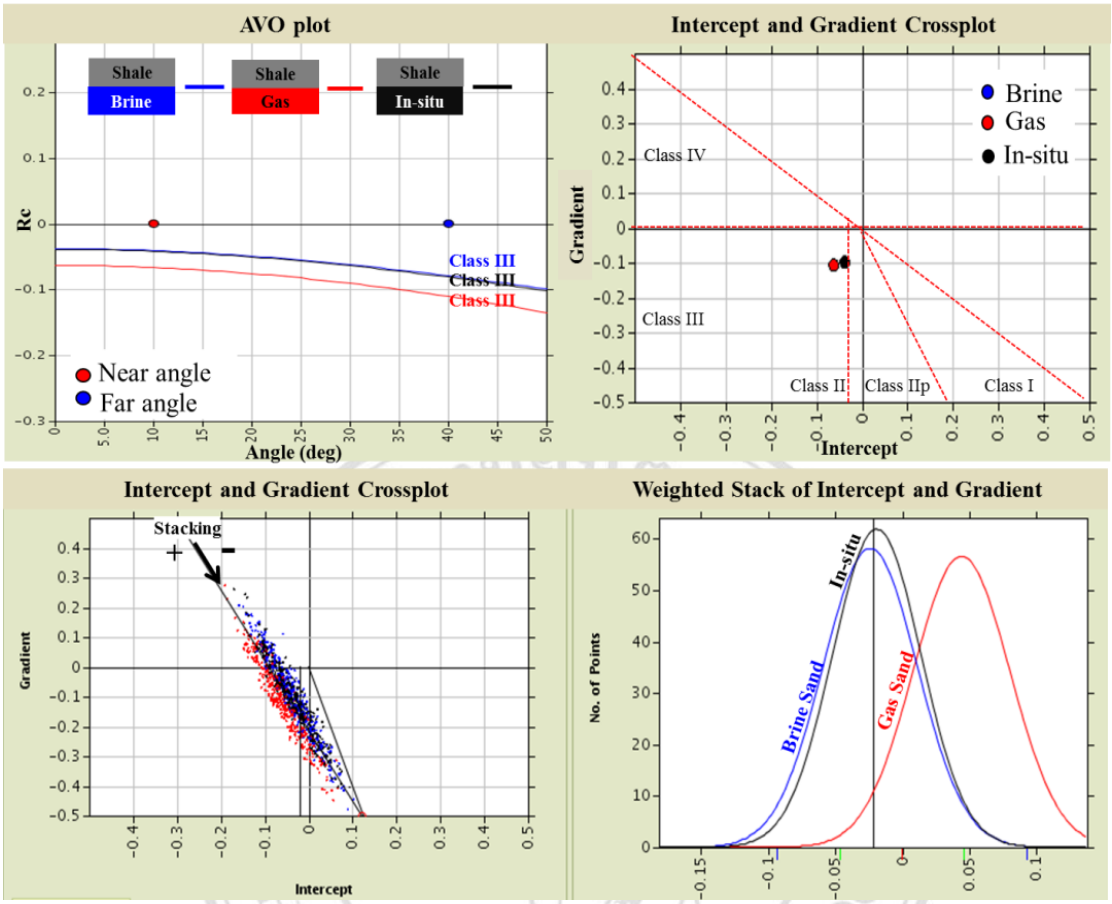

Figure 3-13 The plots using Well-B models for AVO classification comprised (a) AVO analysis plots showing RC versus incidence angle, (b) intercept-gradient crossplot, (c) Monte-Carlo simulation of intercept-gradient at interface with weighted stack function, and (d) a Gaussian distribution of data points based on Monte-Carlo simulation.

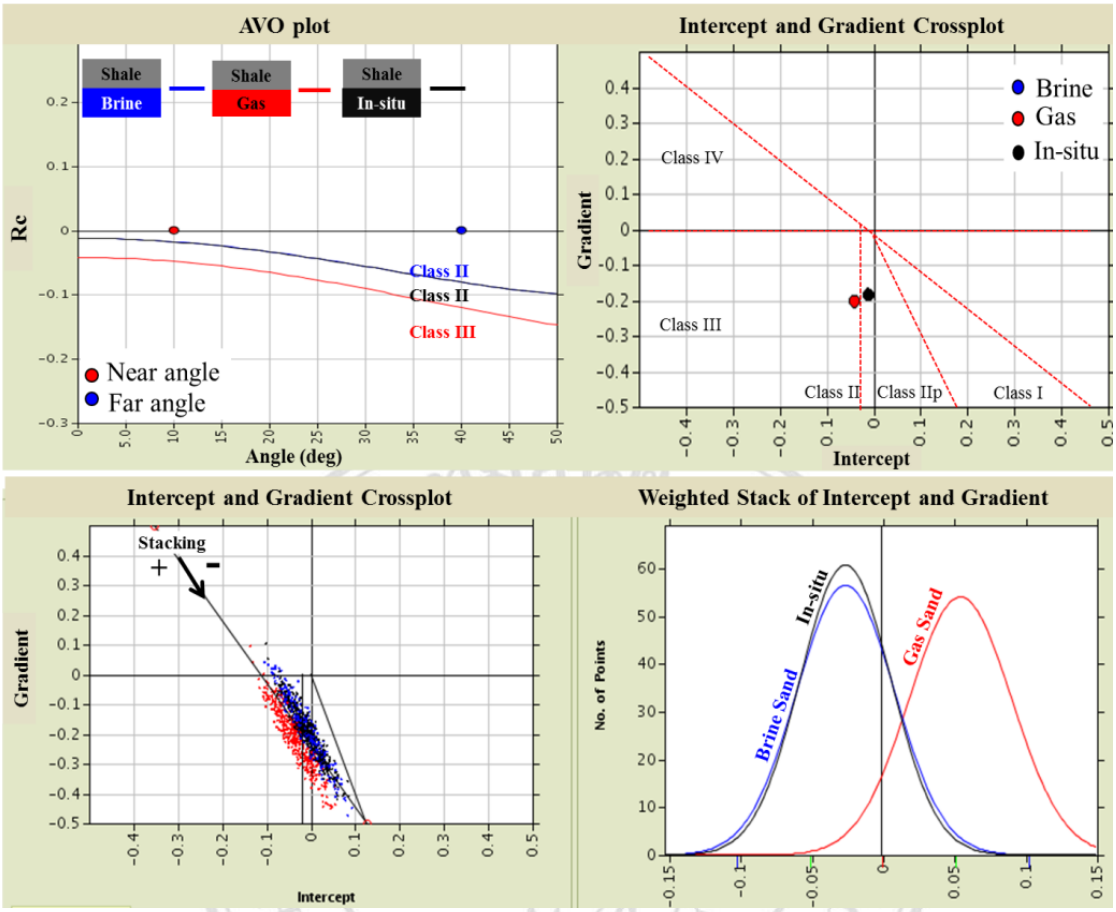

Figure 3-14 The plots using Well-C models for AVO classification comprised (a) AVO analysis plots showing RC versus incidence angle, (b) intercept-gradient crossplot, (c) Monte-Carlo simulation of intercept-gradient at interface with weighted stack function, and (d) a Gaussian distribution of data points based on Monte-Carlo simulation.

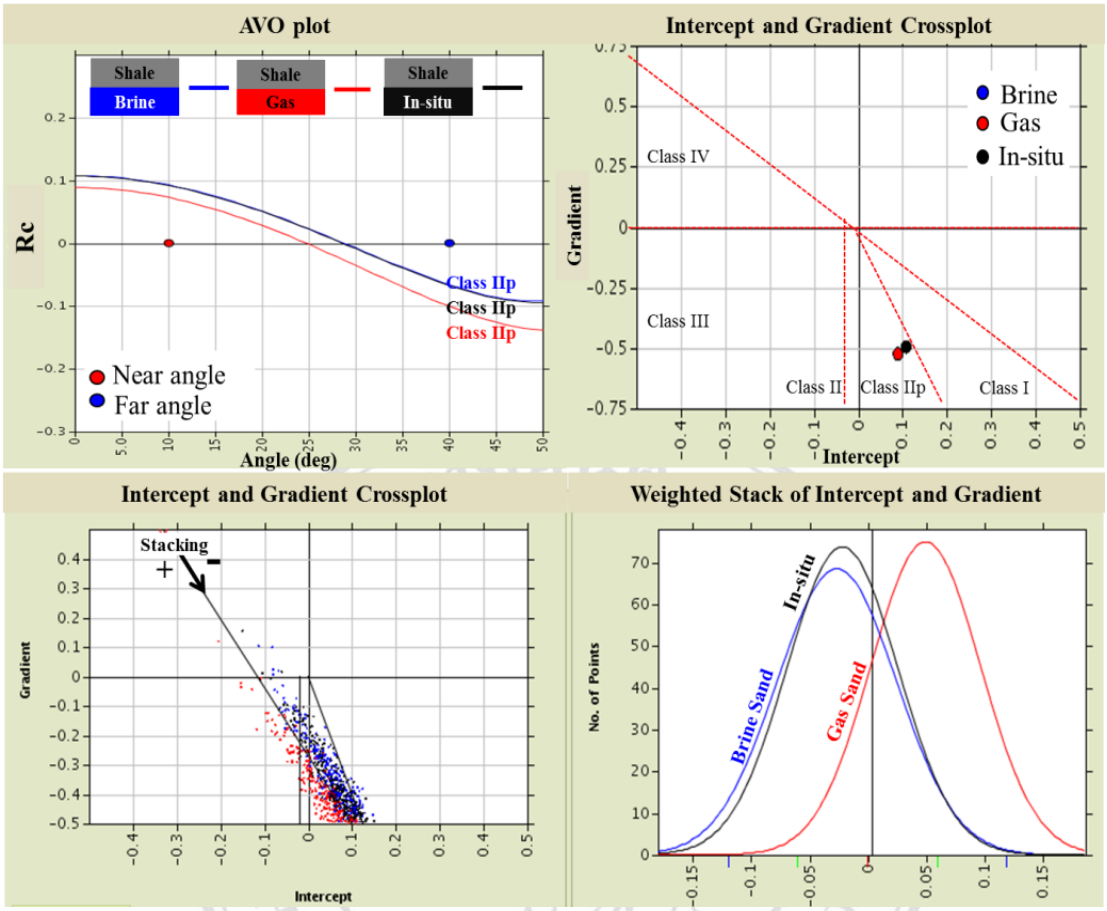

Figure 3-15 The plots using Well-D models for AVO classification comprised (a) AVO analysis plots showing RC versus incidence angle, (b) intercept-gradient crossplot, (c) Monte-Carlo simulation of intercept-gradient at interface with weighted stack function, and (d) a Gaussian distribution of data points based on Monte-Carlo simulation.